J|A|C|S
ARTICLES
Published on Web 11/07/2006

Neutron Diffraction and Simulation Studies of $CsNO_3$ and Cs_2CO_3 Solutions

Philip E. Mason,[†] George W. Neilson,[‡] Christopher E. Dempsey,[§] and John W. Brady*,[†]

Contribution from the Department of Food Science, Stocking Hall, Cornell University, Ithaca, New York 14853, H. H. Wills Physics Laboratory, University of Bristol, BS8 1TL, U.K., and Department of Biochemistry, University of Bristol, BS8 1TD, U.K.

Received March 7, 2006; E-mail: jwb7@cornell.edu

Abstract: Neutron diffraction with isotopic substitution (NDIS) experiments and molecular dynamics (MD) simulations have been used to study the structuring in aqueous solution of two cesium salts, cesium carbonate, and cesium nitrate. As was previously found for guanidinium salts of carbonate, mesoscopic-scale clusters were seen to form in the Cs_2CO_3 solution both in the MD simulations and in the diffraction experiments. No such large scale ion clusters were found in the $CsNO_3$ solutions in either the modeling or experiments. The results are dominated by the strength and geometry of the direct first-neighbor interactions, which explain the differences in the clustering behavior between the two solutions without need to refer to longer-range water−water structuring.

Introduction

The structure of electrolyte solutions has been the subject of intense interest for over a century. Theoretical models of such structuring date back to the pioneering work of Debye and Huckel, while neutron diffraction has been the primary experimental method for probing this structure. A variety of recent studies, including neutron diffraction experiments and MD simulations,[1−4] dynamic light scattering experiments,[5] conductivity measurements,[6,7] and Raman spectroscopy[8,9] have suggested that the distribution of solvated ions in some electrolyte solutions is not uniform. Rather, various degrees of strong ion pairing leading to the formation of extensive nanometer-scale clusters has been suggested. In the case of guanidinium carbonate, the existence of such clusters not only has been predicted by MD simulations and also suggested by neutron diffraction but has been confirmed by small angle neutron scattering (SANS) experiments.[3]

The great advantage of neutron diffraction experiments is that the resulting structure factors are calculated directly from the experimental data and contain information about the correlation of all atoms in the solution to all other atoms. However, these data for aqueous solutions of relatively large molecules have several limitations when used to derive structural information. The first of these limitations is that structure factors are functions of reciprocal space and must be Fourier transformed to yield actual information about real space structure. Another important limitation is that, in the case of even moderately complex systems, such as molecular solutes in molecular solvents, the corresponding complexity of the total scattering function, with its correlation of every atom to every other atom, can itself frustrate attempts to understand these data in terms of actual solution structure. The method of neutron diffraction with isotopic substitution (NDIS) was developed to deal with this complexity. In this method, paired experiments are carried out on twinned systems, in one of which one atomic nucleus type is substituted with an isotope of the same element with a different neutron scattering cross section. By taking the difference in the scattering from these two experiments, all correlations that do not involve the substituted nucleus type cancel, since they will be the same in the two experiments. In the case of a polyatomic solute in water, this procedure still leaves an extremely complicated total atomic radial distribution function consisting of many individual atomic radial distribution functions, each potentially consisting of several peaks and minima at varying distances.

Recent studies of complex aqueous solutions have demonstrated how MD simulations can be used to interpret the peaks observed in neutron diffraction experiments, particularly NDIS experiments, and thus to extract useful information about solution structure from such NDIS experiments.[1−3,10−12] The

[†] Cornell University.
[‡] H. H. Wills Physics Laboratory, University of Bristol.
[§] Department of Biochemistry, University of Bristol.

(1) Mason, P. E.; Neilson, G. W.; Enderby, J. E.; Saboungi, M.-L.; Dempsey, C. E.; MacKerell, A. D.; Brady, J. W. *J. Am. Chem. Soc.* **2004**, *126*, 11462−11470.
(2) Mason, P. E.; Dempsey, C. E.; Neilson, G. W.; Brady, J. W. *J. Phys. Chem. B* **2005**, *109*, 24185−24196.
(3) Mason, P. E.; Neilson, G. W.; Kline, S. R.; Dempsey, C. E.; Brady, J. W. *J. Phys. Chem. B* **2006**, *110*, 13477−13483.
(4) Wahab, A.; Mahiuddin, S.; Hefter, G.; Kunz, W.; Minofar, B.; Jungwirth, P. *J. Phys. Chem. B* **2005**, *109*, 24108−24120.
(5) Georgalis, Y.; Kierzek, A. M.; Saenger, W. *J. Phys. Chem. B* **2000**, *104*, 3405−3406.
(6) Mullin, J. W.; Raven, K. D. *Nature* **1961**, *190*, 251−251.
(7) Mullin, J. W.; Raven, K. D. *Nature* **1962**, *195*, 35−38.
(8) Cerreta, M. K.; Berglund, K. A. *J. Cryst. Growth* **1987**, *84*, 577−588.
(9) Rusli, I. T.; Schrader, G. L.; Larson, M. A. *J. Cryst. Growth* **1989**, *97*, 345−351.
(10) Mason, P. E.; Neilson, G. W.; Enderby, J. E.; Saboungi, M.-L.; Brady, J. W. *J. Phys. Chem. B* **2005**, *109*, 13104−13111.

10.1021/ja0613207 CCC: $33.50

complete atomic and molecular detail available in MD simulations allows individual peaks in the experimental radial distribution functions to be assigned through their correlation with the peaks found in the simulations and to be interpreted in terms of their structural origins using the simulations. Such combined MD and NDIS studies have previously been used to probe the intramolecular conformational structure of carbohydrates[11,12] and to demonstrate that some aqueous electrolyte solutions undergo extensive clustering, leading to the formation of aggregates on the nanometer size scale, while other salts do not.[1−3] In this paper, we again combine the results of MD and NDIS studies of two cesium salts, $CsNO_3$ and Cs_2CO_3, and find that one forms mesoscopic-scale aggregates while the other does not. While such aggregates have previously been observed for the large and complex cation guanidinium, a principal goal of this study was to examine whether such complex cation architectures are necessary for extended ion aggregates to exist.

Methods

Computational Procedures. In the MD simulations, neutral periodic cubic systems were created containing a number of independent cations and anions surrounded by explicit water molecules. Identical methods were used for creating the starting coordinates for both the $CsNO_3$ and Cs_2CO_3 solutions; for brevity only the setup for the $CsNO_3$ starting coordinates will be described in detail. Arbitrary starting coordinates were generated by randomly placing and orienting 24 Cs^+ and 24 NO_3^- ions in a cubic box with sides of 34 Å. These coordinates were then superimposed on a box of 1296 water molecules. Those solvent molecules which overlapped any solute atoms were discarded. By design this procedure produced a 1.4 molal solution (24 $CsNO_3$ in 952 water molecules, 1.4 *m*). Finally the box length was rescaled to 31.3920 Å, which yielded the correct physical number density, 0.0962 atoms $Å^{-3}$. The Cs_2CO_3 box had dimensions of 30.6314 Å, a number density of 0.0977, and contained 24 Cs_2CO_3 molecules and 888 water molecules (1.5 *m*). All simulations were performed using the general molecular mechanics program CHARMM, with chemical bonds to hydrogen atoms kept fixed using SHAKE[13] and a time step of 1 fs. The atomic charges and structures for the CO_3^{2-} and NO_3^- ions were calculated using the GAMESS program[14] at the MP2/6/311G** level using Mulliken assignment (C, 0.676; O, −0.892 (carbonate); N, 0.602; O, −0.534 (nitrate)). These charges are somewhat smaller than the RESP charges for nitrate used in previous AMBER simulations[4,15] but are consistent with the charges used for the carbonate ion,[3] which is important for the direct comparison of the two anions. Water molecules were modeled using either the TIP3P[16] or SPC/E[17] functions. These two water models, which differ in their longer-range structuring, were compared to determine whether the results were affected by the water model and, particularly, whether intermediate-range structuring played an important role in the observed ion clustering.

van der Waals interactions were smoothly truncated on an atom-by-atom basis using switching functions from 10.5 to 11.5 Å,[18] while electrostatic interactions were treated using the Ewald method[19] with a real space cutoff of 12.5 Å, $\kappa = 0.333$ and a K_{max}^2 of 27. Initial velocities were assigned from a Boltzmann distribution (300 K) followed by 5 ps of equilibration dynamics with velocities being reassigned every 0.1 ps. The simulations were then run for 1.3 ns with no further velocity reassignment. The first 0.3 ns of this was taken as equilibration, and the remaining 1 ns was used for analysis. Subsequently, $g_{HH}(r)$, ${}^nG_H^Y(r)$, and ${}^nG_Y^Y(r)$were computed by summing the calculated pair correlation functions, weighted where appropriate by the scattering prefactors shown below. The exact same procedure was repeated using the SPC/E water model instead of TIP3P.

NDIS Experiments. The technique of NDIS is well documented in the literature[20−22] and uses the assumption that solutions of identical chemical constitution, but with different isotopic concentrations of a probe nucleus, are structurally equivalent around the probe nucleus. In this study H/D substitution was performed on solutions of $CsNO_3$ and Cs_2CO_3 to determine three types of structural functions: the correlation of only the hydrogen atoms to other hydrogen atoms; a function containing correlations of the hydrogen nuclei to all other nuclei in the system (other than hydrogen); and finally a function containing information on the structure of all the non-hydrogen atoms relative to all of the other non-hydrogen atoms.

Neutron scattering patterns were obtained from the D4C diffractometer at the Institut Laue Langevin in Grenoble for solutions containing 1.50 mol of Cs_2CO_3 or 1.40 mol of $CsNO_3$ (as dictated by the maximum solubility of $CsNO_3$ in D_2O) in 55.55 mol of water (hereafter referred to as 1.5 *m* Cs_2CO_3, and 1.4 *m* $CsNO_3$), in H_2O, D_2O, and HDO. These solutions were chosen due to their near identical atomic compositions and because the NO_3^- and CO_3^{2-} ions are structurally very similar. The solutions were prepared by direct dissolution of the salts in water. The total raw scattering patterns were measured at 23 °C, corrected for multiple scattering, incoherent scattering, and absorption,[23] and normalized versus a standard vanadium rod to give the $F(Q)$s of each respective solution using literature procedures. $F(Q)$ can be written as

$$F(Q) = \sum_{\alpha}\sum_{\beta} c_\alpha c_\beta b_\alpha b_\beta (S_{\alpha\beta}(Q) - 1) \qquad (1)$$

where c_α is the atomic concentration of species α, whose coherent neutron scattering length is b_α, and the summations are over all four atomic species in the solution. $S_{\alpha\beta}(Q)$ is the partial structure factor of atoms α and β and is directly related to the pair radial distribution function $g_{\alpha\beta}(r)$ through Fourier transformation

$$g_{\alpha\beta}(r) - 1 = \frac{1}{2\pi^2\rho r}\int (S_{\alpha\beta}(Q) - 1) Q \sin(Qr)\, dQ \qquad (2)$$

By taking various differences between the three isotope-dependent $F(Q)$s, it is possible to investigate, at an atomic resolution, the perturbations in the solution structure due to the presence of the two salts.

The method used to extract this information is similar to that used previously in the study of glucose solutions.[10] In this procedure the $S_{HH}(Q)$ is first calculated from the three $F(Q)$s of each solution. The corresponding $g_{HH}(r)$ values of the two solutions were calculated in a self-consistent way by Fourier transformation of $S_{HH}(Q)$ and analyzed to give information on the coordination of one hydrogen atom around other hydrogen atoms. Subsequently, two additional partial structure functions were generated. The first of these, ${}^n\Delta_H^Y(Q)$, was obtained by subtraction of a suitably scaled $S_{HH}(Q)$ from the difference between

(11) Mason, P. E.; Neilson, G. W.; Enderby, J. E.; Saboungi, M.-L.; Brady, J. W. *J. Am. Chem. Soc.* **2005**, *127*, 10991−10998.
(12) Mason, P. E.; Neilson, G. W.; Enderby, J. E.; Saboungi, M.-L.; Brady, J. W. *J. Phys. Chem. B* **2006**, *110*, 2981−2983.
(13) van Gunsteren, W. F.; Berendsen, H. J. C. *Mol. Phys.* **1977**, *34*, 1311−1327.
(14) Schmidt, M. W.; Baldridge, K. K.; Boatz, J. A.; Elbert, S. T.; Gordan, M. S.; Jensen, J. H.; Koseki, S.; Matsunaga, N.; Nguyen, K. A.; Su, S.; Windus, T. L.; Dupuis, M.; Montgomery, J. A. *J. Comput. Chem.* **1993**, *14*, 1347−1363.
(15) Velardez, G. F.; Alavi, S.; Thompson, D. L. *J. Chem. Phys.* **2004**, *120*, 9151−9159.
(16) Jorgensen, W. L.; Chandrasekhar, J.; Madura, J. D.; Impey, R. W.; Klein, M. L. *J. Chem. Phys.* **1983**, *79*, 926−935.
(17) Berendsen, H. J. C.; Grigera, J. R.; Straatsma, T. P. *J. Phys. Chem.* **1987**, *91*, 6269−6271.
(18) Brooks, B. R.; Bruccoleri, R. E.; Olafson, B. D.; Swaminathan, S.; Karplus, M. *J. Comput. Chem.* **1983**, *4*, 187−217.
(19) Darden, T.; York, D.; Pedersen, L. *J. Chem. Phys.* **1993**, *98*, 10089−10092.
(20) Enderby, J. E. *Chem. Soc. Rev.* **1995**, *24*, 159−168.
(21) Neilson, G. W.; Mason, P. E.; Ramos, S.; Sullivan, D. *Philos. Trans. R. Soc. London* **2001**, *A359* (1785), 1575−1591.
(22) Squires, G. L. *Introduction to the Theory of Thermal Neutron Scattering*; Cambridge University Press: Cambridge, 1978.
(23) Barnes, A. C.; Hamilton, M. A.; Beck, U.; Fischer, H. E. *J. Phys.: Condens. Matter* **2000**, *12*, 7311−7322.

the $F(Q)$s of the heavy water and light water samples of each solution. This new function provides information associated with correlations between hydrogen atoms and all other atom types (other than hydrogen) and can be written (for the $CsNO_3$ solution) as

$$ {}^{n}\Delta_H^Y(Q) = \frac{AS_{HOw}(Q) + BS_{HOi}(Q) + CS_{HCs}(Q) + DS_{HN}(Q)}{A + B + C + D} - 1 \quad (3) $$

The superscript Y is used to indicate a sum over all the non-hydrogen atom species. The superscript n indicates that this function is dimensionless, having been normalized by division by the sum of scattering prefactors, in this case $A + B + C + D$. The prefactors themselves are composed of the product $c_\alpha c_\beta b_\alpha \Delta b_H$, where $\Delta b_H = b_D - b_H$. While neutron scattering cannot distinguish chemically different nuclei of the same element, it is useful, as shall be seen later, to further subdivide the oxygen atoms into those on water (Ow) and those on the oxyanion (Oi).

The Fourier transformation of ${}^{n}\Delta_H^Y(Q)$ yields the function ${}^{n}G_H^Y(r)$, which provides information on the pairwise structural correlations between hydrogen atoms and all atoms other than hydrogen in the system. Specifically for the $CsNO_3$ solution:

$$ {}^{n}G_H^Y(r) = \frac{Ag_{HOw}(r) + Bg_{HOi}(r) + Cg_{HCs}(r) + Dg_{HN}(r)}{A + B + C + D} \quad (4) $$

For the 1.5 m* Cs_2CO_3 and 1.4 m* $CsNO_3$ the ${}^{n}G_H^Y(r)$ values were calculated to be, respectively,

$$ {}^{n}G_H^Y(r) = 0.860g_{HOw}(r) + 0.0696g_{HOi}(r) + 0.043g_{HCs}(r) + 0.026g_{HC}(r) \quad (5) $$

and

$$ {}^{n}G_H^Y(r) = 0.877g_{HOw}(r) + 0.0663g_{HOi}(r) + 0.021g_{HCs}(r) + 0.035g_{HN}(r) $$

The second function, ${}^{n}\Delta_Y^Y(Q)$, is obtained by subtraction of a sum of suitably scaled $S_{HH}(Q)$ and ${}^{n}\Delta_H^Y(Q)$ from the heavy water total structure factor of each isotopically labeled solution. This function can be written as (for the $CsNO_3$ solution)

$$ {}^{n}\Delta_Y^Y(Q) = \frac{\begin{array}{l} ES_{OwOw}(Q) + FS_{OwOi}(Q) + GS_{OwCs}(Q) + \\ HS_{OwN}(Q) + IS_{OiOi}(Q) + JS_{OiCs}(Q) + \\ KS_{OiN}(Q) + LS_{CsCs}(Q) + MS_{CsN}(Q) + NS_{NN}(Q) \end{array}}{E + F + G + H + I + J + K + L + M + N} - 1 \quad (6) $$

Fourier transformation of ${}^{n}\Delta_Y^Y(Q)$ gives the function ${}^{n}G_Y^Y(r)$, which contains information on the pairwise correlations between all atoms other than hydrogen.

$$ {}^{n}G_Y^Y(r) = \frac{\begin{array}{l} Eg_{OwOw}(r) + Fg_{OwOi}(r) + Gg_{OwCs}(r) + \\ Hg_{OwN}(r) + Ig_{OiOi}(r) + Jg_{OiCs}(r) + \\ Kg_{OiN}(r) + Lg_{CsCs}(r) + Mg_{CsN}(r) + Ng_{NN}(r) \end{array}}{E + F + G + H + I + J + K + L + M + N} \quad (7) $$

However due to the prefactor weightings ($E-N$), the first four terms of this function, relating to Ow, constitute approximately 98.5% of this measurement. For brevity we will ignore the last six terms. For the $CsNO_3$ and Cs_2CO_3 solutions, respectively,

$$ {}^{n}G_Y^Y(r) \cong 0.770g_{OwOw}(r) + 0.116g_{OwOi}(r) + 0.0362g_{OwCs}(r) + 0.0626g_{OwN}(r) \quad (8) $$

and

$$ {}^{n}G_Y^Y(r) \cong 0.740g_{OwOw}(r) + 0.119g_{OwOi}(r) + 0.0746g_{OwCs}(r) + 0.0458g_{OwC}(r) $$

Notably 100% of the correlations of $g_{HH}(r)$ are due to water−water correlations. About 85% of the function ${}^{n}G_H^Y(r)$ is due to water−water correlations, while about 15% is due to water−ion correlations. About 75% of ${}^{n}G_Y^Y(r)$ is due to water−water correlations, while about 25% of the function is related to the water−ion structure. It is therefore expected that water−ion correlations will be most prominent in ${}^{n}G_Y^Y(r)$, somewhat less prominent in ${}^{n}G_H^Y(r)$, and least prominent in $g_{HH}(r)$.

Results and Discussion

MD Simulations. As was seen previously[3] in studies of aqueous solutions of guanidinium carbonate (Gdm_2CO_3), the Cs_2CO_3 solutions were found to undergo extensive, strong heteroion pairing, which lead to the formation of mesoscopic-scale aggregates with dimensions on the order of 10−15 Å. The $CsNO_3$ solutions, however, exhibited weaker pairing and no formation of aggregates, similar to the behavior previously seen for solutions of GdmSCN[2] and GdmCl.[1] The difference in the behavior of these two solutions is illustrated in Figure 1, which displays typical snapshots from the trajectories for both solutions. As can be seen from this figure, the large aggregates in the Cs_2CO_3 solution have a wormlike structure, with no interior and all ions essentially on the surface and in contact with water. This structure is very similar to that observed previously for Gdm_2CO_3 and Gdm_2SO_4.[2,3]

As in the previous studies of electrolyte solutions, a number of tests were conducted to verify that the observed clustering was not the result of identifiable artifacts of the simulations. To test whether there was any dependence on the water model used, the simulations were repeated using the much more structured SPC/E function, which unlike the TIP3P function exhibits a clear second peak at 4.5 Å in the oxygen−oxygen radial distribution function $g_{OO}(r)$ for pure water. The observation of clustering in the Cs_2CO_3 solution and not in the $CsNO_3$ solution was unaffected by this change. The dependence of the clustering results on the treatment of long-range interactions was tested by repeating the Cs_2CO_3 simulation using different parameters for the particle-mesh Ewald algorithm, again without effect. To test the sensitivity of the ion clustering to the charge assignment of the carbonate ion (that is, how the −2 charge is distributed between the carbon and three oxygen nuclei), this simulation was repeated with a charge of −0.667 on the Oi and 0.00 on the C nuclei. While there was a difference of almost a full formal charge on the C nuclei between these two simulations, only minor changes were found in the level and form of heteroion pairing and the level of ion clustering.

The difference in clustering and aggregation behavior of these two salts is interesting when considered in light of their solubilities in water. It might be expected that the salt which exhibits the most ion pairing would also be the salt with the lower solubility. However, for the cesium salts the opposite trend is observed, with $CsNO_3$, which shows weak ion pairing, having a maximum solubility of about 1.5 m (a low solubility for a nitrate), while the strongly ion-pairing Cs_2CO_3 is soluble up to ca. 8 m (a high maximum solubility for a carbonate). However, since solubility is determined by the difference in chemical potential between the crystal and the solution for each species,

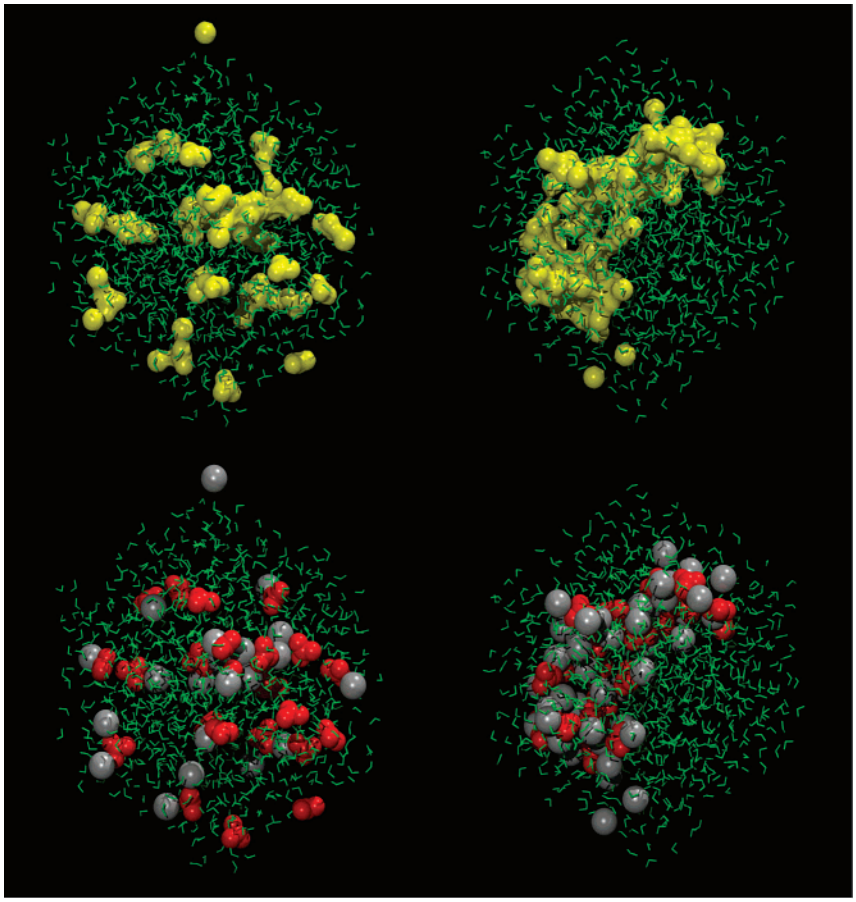

Figure 1. Representative snapshots of the MD simulations of 1.4 molal $CsNO_3$ (left) and 1.5 molal Cs_2CO_3 (right). In the upper representation the water accessible surface of the ions is shown in yellow, while in the lower representation the oxyanions are colored red, and the cesium ions, silver. As can be seen there is extensive ion clustering in the Cs_2CO_3 solution, while in the $CsNO_3$ solution there is almost none.

which includes such factors as differences in lattice energies, it is not possible to make such a simplistic correlation with pairing.

From the MD trajectories the full three-dimensional probability densities for finding the different species around the molecular anions can be calculated and are displayed in Figures 2 and 3. Figure 2 contours the probability of finding water molecule oxygen atoms around both anions. As can be seen from this figure, the carbonate ion structures the water solvent much more strongly than does the nitrate. Because of the stronger and more linear interactions to water made by the carbonate ion, the water molecules are more restricted in their pattern of distribution around the ion, occupying bands of density at approximately −60°, 0°, and 60° with respect to the anionic molecular plane. The hydrogen bonding of the nitrate to the solvent is weaker and more diffuse and resembles a halo centered on the NO bond axis.

Figure 3 displays the densities of other ions around the two molecular anions. As with the water structuring, the cations are much more ordered around the more highly charged carbonate anion. In both cases the cations preferentially occupy positions straddling between adjacent oxygen atoms and in a ring on the top and bottom over the central heavy atom. As can be seen from the pattern of structuring of other anions around a central anion, there is very little longer-range structuring in the nitrate case, as would be expected from the tendency of these ions not to form larger aggregates, while the aggregated character of the carbonate distribution is clearly reflected in the highly ordered arrangement of carbonate ions relative to one another, mediated by the cesium ions.

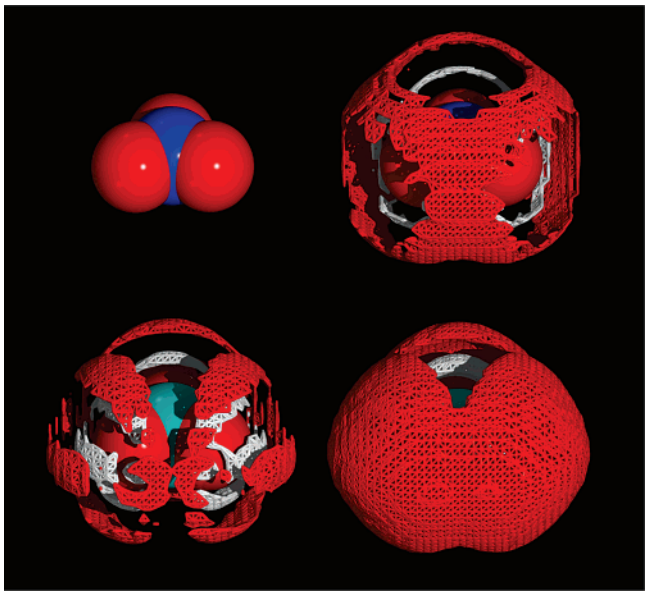

Figure 2. Density maps of water molecules around the NO_3^- (upper) and CO_3^{2-} (lower) ions showing the different strengths and modes by which the waters hydrogen bond to the oxyanion. In all cases the density of Ow is shown in red, and the density of H is shown in white. In all cases the orientation of the species NO_3^-/CO_3^{2-} is identical. The density contours are at number densities of the following: left, Ow 0.25 and H 0.5; right, Ow 0.125, Hw 0.25.

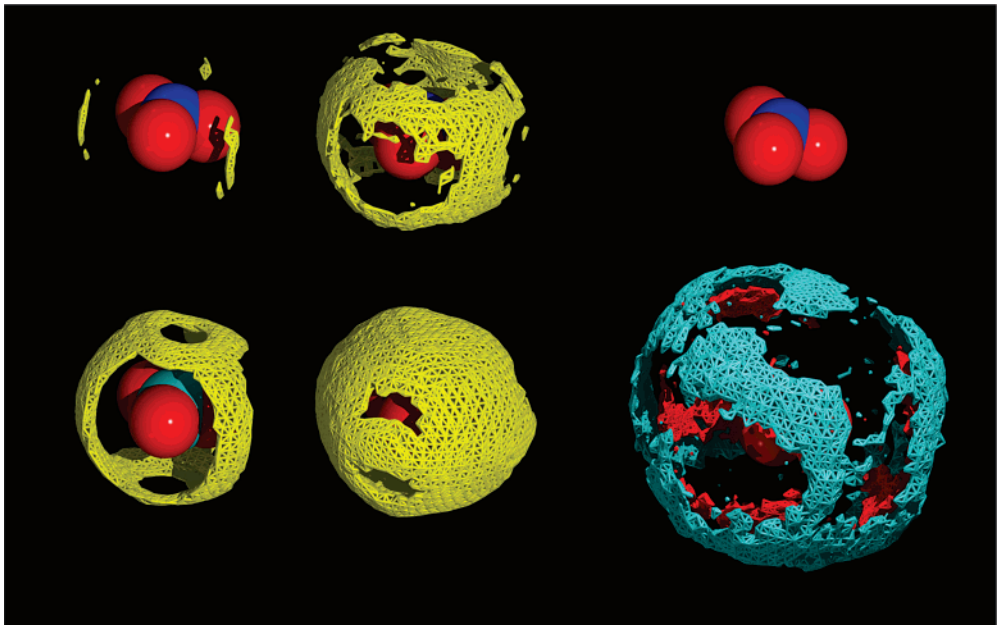

Figure 3. Density maps of ions around the NO_3^- (upper) and CO_3^{2-} (lower) ions. In all cases the oxyanion has the same orientation. The four yellow density maps are Cs^+ around the NO_3^- and CO_3^{2-} ions while both the right density maps are the oxyanion distribution around the NO_3^- and CO_3^{2-} ions (red O_i, cyan C or N, respectively). The Cs^+ density contours are as follows: left (NO_3^-) 0.025, middle (NO_3^-) 0.0075, left (CO_3^{2-}) 0.050, middle (CO_3^{2-}) 0.0150. The right two density maps are (CO_3^{2-}) Oion (red) 0.015, C (cyan) 0.005, and (NO_3^-) Oion (red) 0.015, N (cyan) 0.005.

From the simulations, the experimentally measurable radial atomic pair distribution functions $g_{HH}(r)$, ${}^n G_H^Y(r)$, and ${}^n G_Y^Y(r)$ can be calculated for comparison with the diffraction data. The most useful of these functions for characterizing the overall structure of the solutions is the heavy atom correlation function ${}^n G_Y^Y(r)$, although it is also the most complicated to interpret. This function contains contributions from 10 radial distribution functions, although the components due to $g_{OwOw}(r)$, $g_{OwOi}(r)$, $g_{OwCs}(r)$, and $g_{OwC}(r)$ or $g_{OwN}(r)$ constitute about 98% of ${}^n G_Y^Y(r)$. Figure 4 displays this function from the simulations along with its four principal components for both solutions. As can be seen, the ${}^n G_Y^Y(r)$ functions for these two solutions are very similar, even though their qualitative organization is very different, with one exhibiting strong heteroion pairing and extensive aggregation while the other exhibits very weak heteroion pairing and no aggregation. The crucial differences in ${}^n G_Y^Y(r)$ for the two solutions resulting from their very different organization are sufficiently small that they can best be usefully observed in one of two ways. The first of these is to examine the structures of the individual component functions $g_{OwOw}(r)$, $g_{OwOi}(r)$, $g_{OwCs}(r)$, and $g_{OwC}(r)$ or $g_{OwN}(r)$ contributing to the function ${}^n G_Y^Y(r)$, as is shown in Figure 4, something that is of course only possible for simulation data. As can be seen, the first peak in the $g_{OwOi}(r)$ component, arising from water molecules hydrogen bonded to the oxyanion, is much sharper for the CO_3^{2-} solution than for the NO_3^-. Also, the first peak in $g_{OwCs}(r)$ has about twice the intensity in the CO_3^{2-} solution as that in the NO_3^-, reflecting the fact that this solution has twice the concentration of cesium. However, the most significant difference between the two solutions is in the longer-range ordering, which is apparent in the minor features in ${}^n G_Y^Y(r)$ above about 5 Å in the Cs_2CO_3 but not in the $CsNO_3$ case. Although small, these features are due to the longer-range ion−ion ordering observed in the MD simulations for the Cs_2CO_3 solution which was not found in the $CsNO_3$ solution. About 50% of this longer-range structure for $r > 5$ Å is from the $g_{OO}(r)$ function, and about 50% is from ion−water terms. The small prefactor weightings for the structure factors of the ion−ion terms mean that these do not significantly contribute to the function ${}^n G_Y^Y(r)$ and are essentially unobserved. However, the interpenetrating networks of wormlike nanometer-scale ion aggregates and the surrounding nearly pure water network leave a structural signature on the water−water and water−ion terms in the Cs_2CO_3 solution but not in the $CsNO_3$ case.

The other way to observe the differences between the ${}^n G_Y^Y(r)$ functions for the two solutions is to examine the difference function between the ${}^n G_Y^Y(r)$ for the carbonate and nitrate solutions, $\Delta G_Y^Y(r) = {}^n G_Y^Y(r)_{(Cs_2CO_3)} - {}^n G_Y^Y(r)_{(CsNO_3)}$, shown in Figure 6. Two principal differences are found at $r <$ 4 Å, due to water molecules interacting directly with the ions and longer-range ordering that has peaks at 5.5 and 8.5 Å and relates to the strong ion pairing that occurs in the Cs_2CO_3 but not in the $CsNO_3$.

NDIS Experiments. Three distribution functions were determined in the present experiments, $g_{HH}(r)$, ${}^n G_H^Y(r)$, and ${}^n G_Y^Y(r)$. The heavy atom structure factors ${}^n \Delta_Y^Y(Q)$ and radial distribution functions ${}^n G_Y^Y(r)$ are shown in Figures 5 and 6. Although ${}^n G_Y^Y(r)$ is the most complicated of these functions, it contains the most information about the long-range ordering. These data were corrected for a Placzek effect arising from the large incoherent scattering cross section of ^1H using standard procedures such as those described in the Supporting Information.

From the direct comparison of the experimentally measured ${}^n \Delta_Y^Y(Q)$ and ${}^n G_Y^Y(r)$ functions, it can be seen that the differences between these functions for the two electrolyte solutions are small, as is also the case for the functions calculated from the MD simulations. In comparing the calculated functions to the experimental ones for each solution, it can be seen that the discrepancies are 2 to 3 times larger than the differences between the MD ${}^n G_Y^Y(r)$ functions for the $CsNO_3$ and Cs_2CO_3 solutions,

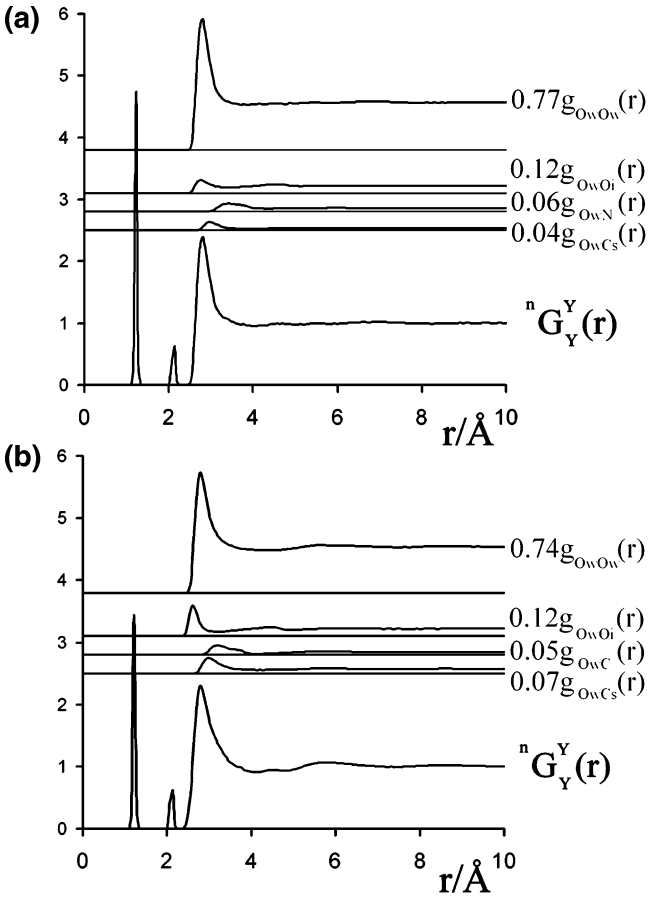

Figure 4. $^{n}G^{Y}_{Y}(r)$ calculated from the MD trajectory. The formats for figures (a) 1.4 *m* $CsNO_3$ and (b) 1.5 *m* Cs_2CO_3 are identical. In each case the function $^{n}G^{Y}_{Y}(r)$ is shown lowest with the principal components above. The four principal components are arranged from top to bottom as $g_{OwOw}(r)$, $g_{OwOi}(r)$, $g_{OwC}(r)$ or $g_{OwN}(r)$ (depending on whether the solution in question is $CsNO_3$ or Cs_2CO_3), and $g_{OCs}(r)$. These four components compose about 98% of the function $^{n}G^{Y}_{Y}(r)$. While these functions are very similar, there are significant differences that result from the nanometer length scale ion clustering that occurs in Cs_2CO_3 solution but not in $CsNO_3$ (Figure 1).

which exhibit almost as large a qualitative difference in actual solute−solute structure as is physically possible. Since the calculated $^{n}G^{Y}_{Y}(r)$ functions are exact for the simulations, this finding would suggest that the weak sensitivity of these total radial distribution functions to such major structural differences presents a significant challenge for diffraction experiments.

Actually the MD simulations are reasonably successful at reproducing the experimental ion−ion ordering signatures in the two solutions, but due to the small absolute differences in the measured functions for the two solutions, a more sensitive comparison of the experimental and modeling data is needed to highlight the success of the modeling. It should be remembered that both the experimental and modeling data contain systematic errors but that these arise from different sources. For example, the experimental data suffer from resolution and scattering artifacts which are not present in the simulations, while a number of approximations such as limitations in the force fields and the treatment of long-range interactions affect the calculated functions but are of course not present in the experimental data. Many of these effects might be expected to be very similar between the two experiments and between the two simulations, so that the difference of the $^{n}\Delta^{Y}_{Y}(Q)$ and $^{n}G^{Y}_{Y}(r)$ functions between the two experiments and between the

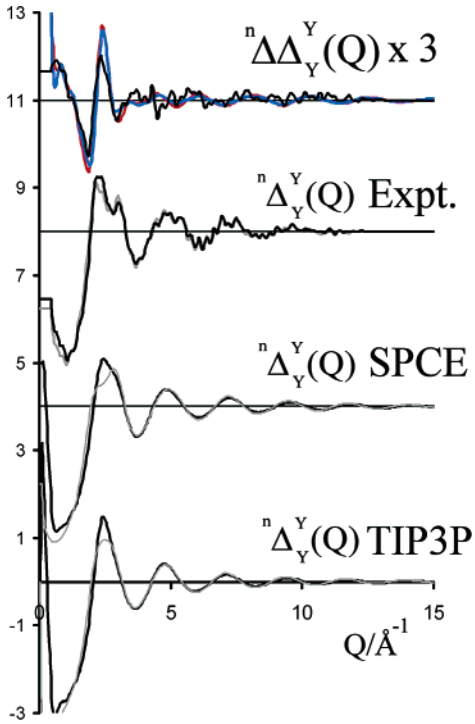

Figure 5. Comparison of the Q-space data. The lower plot is the MD predictions for $^{n}\Delta^{Y}_{Y}(Q)$ in TIP3P water, the lower middle is the MD predictions for $^{n}\Delta^{Y}_{Y}(Q)$ in SPC/E water, and the upper middle plot is the NDIS experimental measurement for $^{n}\Delta^{Y}_{Y}(Q)$, with gray representing $CsNO_3$ and black representing Cs_2CO_3. The upper plot is the difference function $^{n}\Delta\Delta^{Y}_{Y}(Q)$ for Cs_2CO_3 minus $CsNO_3$; blue is from the MD using TIP3P, red is the MD using SPC/E water, and black is from the NDIS measurement. This differential function $^{n}\Delta\Delta^{Y}_{Y}(Q)$ is scaled by a factor of 3.

two simulations should be very similar. As can be seen from Figure 6, the comparison of the $\Delta G^{Y}_{Y}(r)$ functions from experiment and the MD simulations gives excellent agreement.

This comparison is most informative for the structure factor difference function, $^{n}\Delta\Delta^{Y}_{Y}(Q) = {}^{n}\Delta^{Y}_{Y}(Q)(Cs_2CO_3) - {}^{n}\Delta^{Y}_{Y}(Q)(CsNO_3)$ (Figure 5). The most significant signature for intermediate-range ion ordering will be at low *Q*. Accordingly, the good fit of the MD data to those of the experiment in the low *Q* range (0−2 Å^{-1}) is direct experimental evidence that a longer-range structure, of the type suggested by the MD, exists in Cs_2CO_3 but not in $CsNO_3$.

It is interesting to note that the difference between the structuring of these two solutions is observed in both the TIP3P and SPC/E simulations, even though the TIP3P model gives a less structured pure bulk phase than does SPC/E, with only a weak second peak in $g_{OwOw}(r)$ at 4.5 Å. If the functions $^{n}\Delta^{Y}_{Y}(Q)$ and $^{n}G^{Y}_{Y}(r)$ are compared for the TIP3P and SPC/E simulations, significant differences are observed due to the difference between the long-range water structuring in the two simulations, but the difference function $^{n}\Delta\Delta^{Y}_{Y}(Q)$ for the two SPC/E solutions is almost exactly the same as that for the two TIP3P solutions, since the long-range structuring cancels out in comparing the differences, and only the ion pairing signature remains. This is because the dominant effect in determining clustering is the competition between the strong water−ion and ion−ion interactions in the two cases, which makes a much greater contribution to the total energy difference than that resulting from the longer-range water structuring.

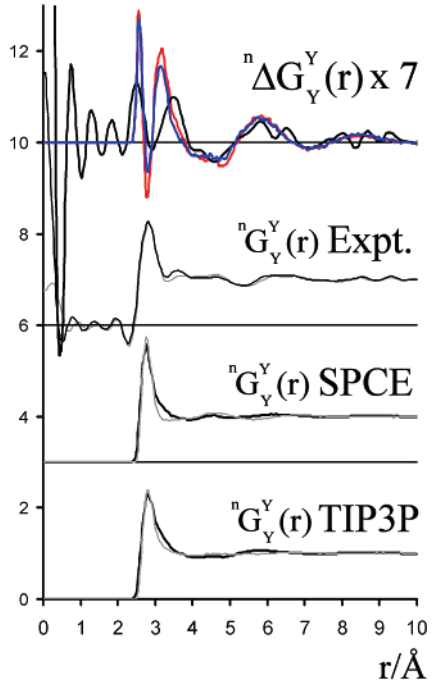

Figure 6. The *r*-space data. In both cases all components relating to structures of *r* range 0 to 2.2 Å have been removed according to procedures described in the manuscript. The lower plot is the MD predictions for $^{n}G^{Y}_{Y}(r)$ in TIP3P water, the lower middle is the MD predictions for $^{n}G^{Y}_{Y}(r)$ in SPC/E water, and the upper middle plot is the NDIS experimental measurement for $^{n}G^{Y}_{Y}(r)$, with gray representing $CsNO_3$ and black representing Cs_2CO_3. The upper plot is the difference function $^{n}\Delta G^{Y}_{Y}(r)$ for Cs_2CO_3 minus $CsNO_3$; blue is from the MD using TIP3P, red is the MD using SPC/E water, and black is from the NDIS measurement. This differential $^{n}\Delta G^{Y}_{Y}(r)$ is scaled by a factor 7.

The first peaks, in the range 0−4 Å, in the total radial distribution functions shown in Figure 6 also contain useful information relevant to the difference in organization in the two solutions. The greater intensity in $^{n}G^{Y}_{Y}(r)$ at 2.6 Å in the carbonate solution is the direct consequence of the stronger hydrogen bonds formed between the water molecules and the CO_3^{-2} ions than those formed to the NO_3^{-} ions. The feature was found to be sharper in the MD simulations than in the NDIS measurements, which is somewhat resolution-limited in the experimental function. The discrepancy between the MD and experimental results is more significant in the peak at 3.5 Å, which arises from correlations between the anion oxygen atoms and those in water and from cesium−oxygen correlations. The source of this discrepancy is unclear, but it may arise from errors in the MD representation of the cesium−oxygen interaction using a nonpolarizable point charge model. However, these inaccuracies do not prevent the MD simulations from distinguishing the levels of ion pairing in the two electrolyte solutions.

Figure 7 displays both the experimental and MD structure factors $^{n}\Delta^{Y}_{H}(Q)$ and radial distribution functions $^{n}G^{Y}_{H}(r)$ for these solutions. The radial distribution function $^{n}G^{Y}_{H}(r)$ contains only four correlations between hydrogen and all other nonhydrogen atoms. This function is very similar for the two electrolyte solutions, both in the experiments and in the MD simulations. As was the case for the heavy atom correlations, the difference between the MD and experimental $^{n}G^{Y}_{H}(r)$ functions for either solution is greater than the difference between the TIP3P and SPC/E simulations for the corresponding salt. As before, this discrepancy is largely due to the inherently

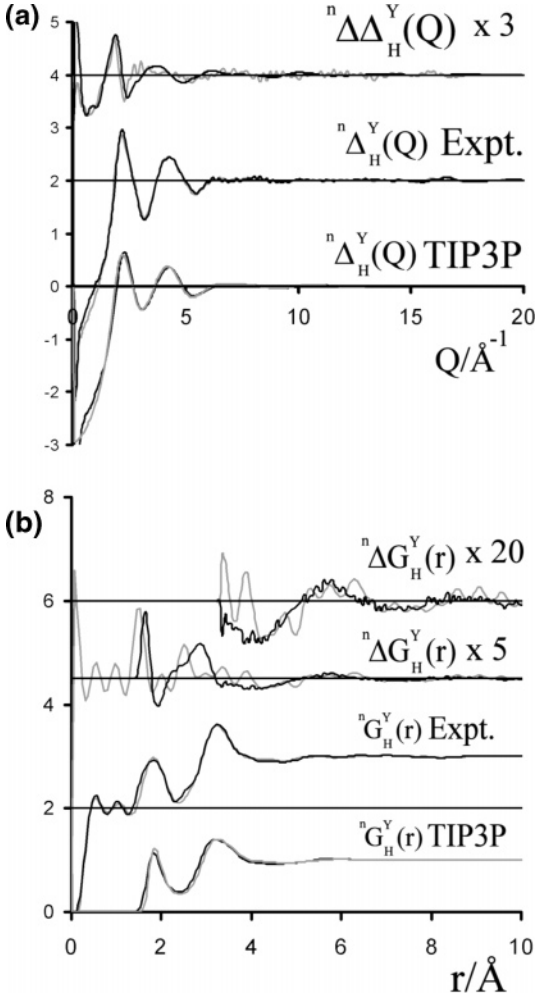

Figure 7. In all cases all components relating to structures in the *r* range 0−1.2 Å have been removed. (a) $^{n}\Delta^{Y}_{H}(Q)$, (b) $^{n}G^{Y}_{H}(r)$. In each case the lower plot is the MD predictions, the middle plot is the NDIS experimental measurement, with gray representing $CsNO_3$ and black representing Cs_2CO_3. The upper plot in each case is the difference function ($^{n}\Delta\Delta^{Y}_{H}(Q)$ or $^{n}\Delta G^{Y}_{H}(r)$) between Cs_2CO_3 and $CsNO_3$; in each case black is from the MD while gray is from the NDIS measurement. This differential function is scaled by a factor of 3 for (a), while the two difference plots for (b) are scaled by 5 and 20 for the lower and upper plot, respectively.

weaker long-range structuring in TIP3P water. Nevertheless, the agreement in the comparison of the difference functions $^{n}\Delta G^{Y}_{H}(r)$ and $^{n}\Delta\Delta^{Y}_{H}(Q)$ is very good, although not as good as for the $^{n}\Delta G^{Y}_{Y}(r)$ and $^{n}\Delta\Delta^{Y}_{Y}(Q)$ cases. Also as before, these differences can be broken down into two separate regimes, one involving distances corresponding to water molecules interacting directly with the ions and one involving longer-range interactions. The longer-range structure above 5.5 Å is predicted well, although not as well as in the case of $^{n}\Delta G^{Y}_{Y}(r)$, but this is in part due to the fact that there is less signal in this structure factor. The structure factors relating to ion−water oxygen correlations contribute approximately 25% to $^{n}\Delta G^{Y}_{Y}(r)$ but only 15% to $^{n}G^{Y}_{H}(r)$.

The functions $g_{HH}(r)$ and the associated structure factors are shown in Figure 8. As with the other functions, it can be seen that the $g_{HH}(r)$ functions for both the $CsNO_3$ and Cs_2CO_3 solutions are very similar for the NDIS experiments, and the same is true for the MD simulations. The function $g_{HH}(r)$ contains information only about the hydrogen atoms of the water molecules and no direct information about the ion structuring.

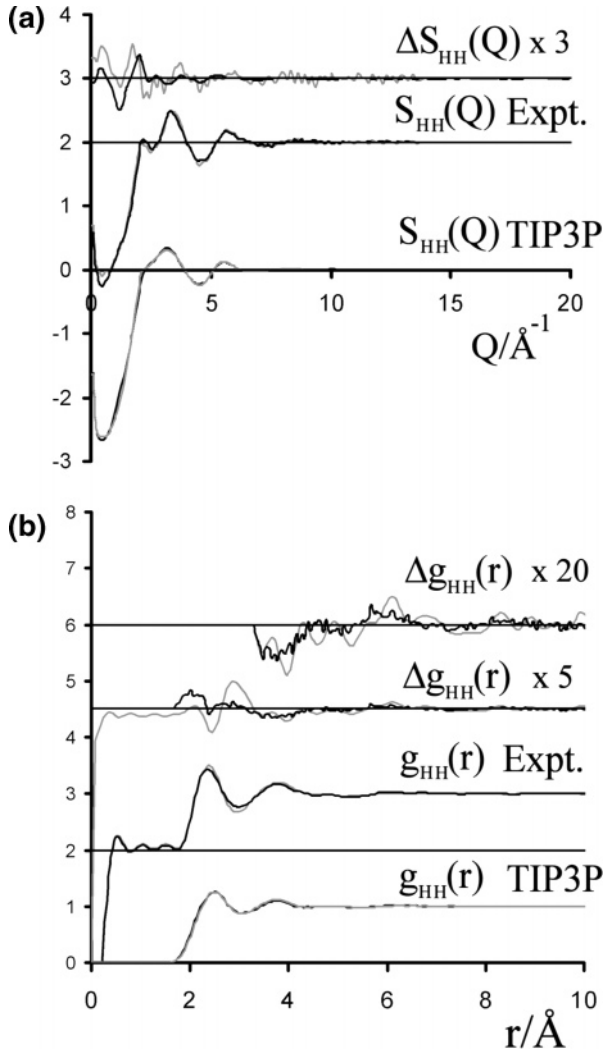

Figure 8. The intramolecular water peak at 1.5 Å has been removed from all data here using a method similar to that described in the Supporting Information. (a) *Q*-space data, (b) *r*-space data. In each case, the lower plot is the MD predictions, and the middle plot is the NDIS experimental measurement (for either $g_{HH}(r)$ or $S_{HH}(Q)$), with gray representing $CsNO_3$ and black representing Cs_2CO_3. The upper plot in each case is the difference function between Cs_2CO_3 and $CsNO_3$ ($\Delta g_{HH}(r)$ or $\Delta S_{HH}(Q)$); in each case black is from the MD, while gray is from the NDIS measurement. This differential function is scaled by a factor of 3 for (a), while the two difference plots for (b) are scaled by 5 and 20 for the lower and upper plot, respectively.

This function exhibits the smallest signature of the long-range ion ordering, and the agreement between the experiments and simulations is significantly worse for the short-range structure below about 3 Å. This result is not unexpected given that in addition to thermal broadening there is quantum uncertainty in the hydrogen atom positions in the experiment and since water bonds are fixed in length in the simulations, which are strictly classical and thus are less able to reproduce the behavior of these inherently quantum mechanical nuclei.

Conclusions

In the studies reported here MD simulations have been used to interpret the scattering data from NDIS experiments for two different aqueous solutions of cesium salts, $CsNO_3$ and Cs_2CO_3, as a probe of the factors which lead to mesoscopic-scale aggregation structures in electrolyte solutions. Previous studies have found that some ion pairs lead to extensive clustering in solution, while others do not,[1−3] a finding that was confirmed by small angle neutron scattering experiments. Similar intermediate-range structuring (on the order of 1.5 nm) has been inferred from experimental studies of several other electrolytes.[5−9] In the present case, these two particular salts were chosen for study because the anions are structurally very similar yet differ by a full electron charge unit in their charge valency. Cesium was chosen as the cation since it has the lowest surface charge density of the monovalent cations. As a structureless atom, it also allowed a test of whether aggregation requires the complex molecular architecture of the guanidinium that was the cation in both of the electrolytes which were previously found to cluster.

As was seen in the previous studies of guanidinium salts, where it was found that Gdm_2SO_4 and Gdm_2CO_3 form extended nanometer-scale aggregates in aqueous solutions while GdmCl and GdmSCN do not, the Cs_2CO_3 studied here exhibited extensive clustering behavior in the MD simulations, while the $CsNO_3$ did not. In the studies reported here the signal for strong ion pairing seen in the MD radial distribution function is reproduced in the experimental data, supporting the validity of the modeling. This aggregation was further found to be robust and not dependent on the water model and anion force field employed. The extensive ion clustering found in the Cs_2CO_3 simulations cannot be seen directly in the Cs_2CO_3 NDIS data, although it can be inferred indirectly from the consequences of the ion pairing observed in the experiment, providing support for the modeling results. However, the observation of nanometer-scale aggregates resulting from the ion pairing stands as a prediction to be further confirmed by future direct methods, such as small angle neutron scattering.

The results indicate that the double hydrogen bonding capacity of the planar NH_2 groups of the guanidinium ions are not a requirement for aggregation. The divalent oxyanions such as SO_4^{-2} and CO_3^{-2}, with their polydentate architectures, seem to have a propensity to form extended aggregates. These results would seem to further support the previous assertion that such differences in direct ionic interactions play an important mechanistic role in determining the relative Hofmeister ordering of ions,[2] rather than their effects on the longer-range structuring of the surrounding water. As the heteroion coordination number of both ions approaches 2, extended ion structuring becomes topologically inevitable. To gain an understanding of extended ion structures it is therefore necessary to understand the factors that lead to high heteroion coordination numbers.

It is interesting that the MD simulations are able to capture the essential signatures of the ion pairing, and do an excellent job of reproducing the experimental data, when compared as difference plots (i.e., when comparing the difference between the MD simulations for the two electrolyte solutions with the difference between the two NDIS experiments), even though the differences between the experiments and simulations are somewhat greater when they are compared directly. This good agreement probably results from the fact that both the experiments and simulations suffer from systematic errors from a number of sources which are different for the two types of studies, but which will be similar between the two experiments or the two calculations. As a result, many of the effects of these systematic errors apparently cancel out when the results are subtracted in the difference functions. This effect can be

observed directly in the case of the MD simulations, where some of these errors can be directly controlled, as for example by substituting one water model for another, as was done here in the SPC/E versus TIP3P comparison. One of the most significant differences between these two water models is in their intermediate-range bulk water structuring, which is reflected in the difference function between these two types of simulations. While the "water structure" for the pure TIP3P and SPC/E models are significantly different, in the difference plot $\Delta G(r)$ this difference largely cancels out. However in both Cs_2CO_3 simulations (TIP3P and SPC/E) there is a similar level of ion pairing/clustering, while in both the $CsNO_3$ cases the ions are similarly homogeneously distributed, with the "water structure" reflecting the ion−ion structure through a reciprocal relationship. Consequentially, it was observed that the difference function $\Delta G(r)$ strongly reflects the difference in the intermediate range ion ordering between the two cesium salts but was not significantly dependent upon the choice of water model.

Acknowledgment. The authors gratefully acknowledge the assistance of G. Cuello and P. Palleau of the ILL. This project was supported by Grant GM63018 from the National Institutes of Health and by the National Science Foundation under Agreement DMR-9986442. The authors thank J. E. Enderby and M.-L. Saboungi for helpful discussions.

Supporting Information Available: A description of the procedures used to correct for the Placzek effect arising from incoherent scattering by ^1H. This material is available free of charge via the Internet at http://pubs.acs.org.

JA0613207